

Photoelectrochemical Conversion from Graphitic C₃N₄ Quantum Dot Decorated Semiconductor Nanowires

Tianc An,^{†,‡} Jing Tang,^{†,‡} Yueyu Zhang,[‡] Yingzhou Quan,[†] Xingao Gong,[‡] Abdullah M. Al-Enizi,[§] Ahmed A. Elzatahry,^{||} Lijuan Zhang,^{*,†} and Gengfeng Zheng^{*,†}

[†]Laboratory of Advanced Materials, Department of Chemistry, Collaborative Innovation Center of Chemistry for Energy Materials, Fudan University, Shanghai 200433, China

[‡]Key Laboratory of Computational Physical Sciences, Ministry of Education, State Key Laboratory of Surface Physics, and Department of Physics, Fudan University, Shanghai 200433, China

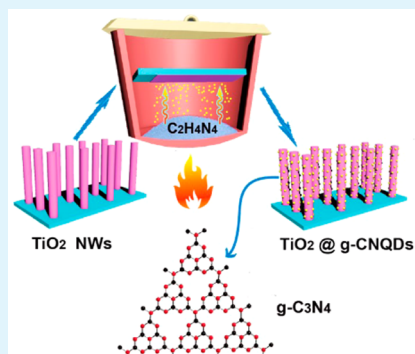
[§]Department of Chemistry, College of Science, King Saud University, Riyadh 11451, Saudi Arabia

^{||}Materials Science and Technology Program, College of Arts and Sciences, Qatar University, Doha, Qatar

Supporting Information

ABSTRACT: Despite the recent progress of developing graphitic carbon nitride (g-C₃N₄) as a metal-free photocatalyst, the synthesis of nanostructured g-C₃N₄ has still remained a complicated and time-consuming approach from its bulk powder, which substantially limits its photoelectrochemical (PEC) applications as well as the potential to form composites with other semiconductors. Different from the labor-intensive methods used before, such as exfoliation or assistant templates, herein, we developed a facile method to synthesize graphitic C₃N₄ quantum dots (g-CNQDs) directly grown on TiO₂ nanowire arrays via a one-step quasi-chemical vapor deposition (CVD) process in a homemade system. The as-synthesized g-CNQDs uniformly covered over the surface of TiO₂ nanowires and exhibited attractive photoluminescence (PL) properties. In addition, compared to pristine TiO₂, the heterojunction of g-CNQD-decorated TiO₂ nanowires showed a substantially enhanced PEC photocurrent density of 3.40 mA/cm² at 0 V of applied potential vs Ag/AgCl under simulated solar light (300 mW/cm²) and excellent stability with ~82% of the photocurrent retained after over 10 h of continuous testing, attributed to the quantum and sensitization effects of g-CNQDs. Density functional theory calculations were further carried out to illustrate the synergistic effect of TiO₂ and g-CNQD. Our method suggests that a variety of g-CNQD-based composites with other semiconductor nanowires can be synthesized for energy applications.

KEYWORDS: carbon nitride quantum dot, TiO₂ nanowires, chemical vapor deposition, photoluminescence, photoelectrochemical conversion



INTRODUCTION

As an attractive metal-free photocatalyst and electrocatalyst, semiconductor graphitic carbon nitride (g-C₃N₄) has been studied extensively for electrochemical water splitting¹ and solar energy conversion applications,² due to its proper band gap edge (~2.7 eV), visible-light absorption, and environmental benignity.³ Bulk g-C₃N₄ can be prepared via a thermal polycondensation of organic precursors rich in nitrogen such as melamine and dicyandiamide,⁴ but the potential polymeric layer stacking from this process often results in a limited surface area and fast recombination of photogenerated electrons and holes, which subsequently leads to relatively low photocatalytic activity.^{5–7} In order to settle these challenges, many studies have been focused on developing nanostructured g-C₃N₄, such as nanosheets,^{8,9} nanospheres,^{10,11} or quantum dots (QDs),¹² while at the same time maintaining their sp² C–N cluster of conjugated tri-s-triazine structures, so as to regulate photoluminescence properties and improve the photoelectrochemical

performances.¹³ Two bottom-up methods are mostly employed in preparing nanostructured g-C₃N₄. The first one involves the exfoliation of bulk g-C₃N₄ using mechanical and solvent approaches,^{14,15} while it typically consists of long hours of sonication or grinding as well as acid or salt treatment. The second method is to use assisted templates such as silica nanostructures for hard templates¹⁶ and Pluronic P123 for soft templates¹⁷ but requires the removal of templates. Thus, developing a facile strategy to synthesize nanostructured g-C₃N₄ is of vital importance to further developing its catalytic mechanism and potential applications.

As a unique nanostructure, QDs have excellent structural, optical, and electronic properties.¹⁸ Previously, carbon QDs and graphene QDs have been widely demonstrated as fluorescent

Received: February 4, 2016

Accepted: May 5, 2016

Published: May 5, 2016

carbon-based materials in cellular bioimaging and also sensitizers in PEC energy conversion.^{19–21} Recently, the graphitic carbon nitride quantum dot (g-CNQD) has also emerged as a potential candidate of carbon-based QDs but with unique photoluminescence (PL) properties that are different from other carbon-based QDs.²² Due to the quantum effect, g-CNQD has a wider band gap than bulk g-C₃N₄ and presents superior catalytic activity as the conduction and valence bands shift in opposite directions, which causes a significant difference in the photophysical properties and photoexcited charge carriers.²³ However, up to now, there have been limited reports about the application of graphitic carbon nitride quantum dots (g-CNQDs). For example, g-CNQDs were successfully synthesized by liquid exfoliation for two-photon fluorescence imaging of cellular nuclei.²² Zhang and co-workers reported the synthesis of nanostructured g-C₃N₄ with versatile morphology and distinct photoluminescence properties from bulk powder of g-C₃N₄.²³ Nonetheless, both preparation methods require intricate synthesis procedures such as acid treatment and sonication to cleave the bulk g-C₃N₄ into QDs. To date, the applications of g-CNQDs have still been limited.

Herein, we developed a facile quasi-chemical vapor deposition (CVD) method using dicyandiamide (C₂H₄N₄) as a precursor to synthesize g-CNQDs, and TiO₂ nanowire (NW) arrays were used to facilitate the deposition of g-CNQDs as well as serve as a semiconductor photoanode material (Figure 1a). As TiO₂ is one of the most attractive photoelectrodes

being explored extensively for energy applications,^{24–26} the combination of TiO₂ NW arrays and g-C₃N₄ QDs with different heterogeneous structures is promising as an effective means to improve the PEC performance of both single components through a synergistic effect. The as-synthesized g-CNQDs exhibited outstanding photoluminescence properties and further served as photosensitizers and stabilizers on the TiO₂ NWs surface. As shown in Figure 1b, the g-CNQD-decorated TiO₂ (designated as TiO₂@g-CNQD) displays a Z-scheme heterojunction according to previous literature.²⁷ When irradiated by light, the photogenerated electrons in TiO₂ with a less-negative conduction band (CB) tend to transfer to g-CNQD with a less-positive valence band (VB) via the contact interface and are further excited to the CB of g-CNQD.³ Compared to unfunctionalized (pristine) TiO₂ NW arrays, the composite TiO₂@g-CNQD exhibited substantially enhanced PEC performance ($\sim 3.40 \text{ mA/cm}^2$ at 0 V vs Ag/AgCl, i.e. 1 V vs reversible hydrogen electrode, RHE), as well as better stability under simulated solar light (300 mW/cm^2), suggesting that this convenient synthesis method of g-CNQD can be used to form composites with other semiconductor nanomaterials.

RESULTS AND DISCUSSION

The TiO₂ NWs were first grown on a transparent fluorine-doped tin oxide (FTO) substrate via a simple solvothermal procedure²⁸ and then used to facilitate the condensation of g-CNQDs through the quasi-CVD process (Methods in the Supporting Information) as shown in Figure S1a. Different from the liquid-assisted method that results in the full coating of the whole growth substrate,²⁹ as the temperature goes up quickly during the CVD process, dicyandiamide solid evaporates and decomposes into small molecules. These molecules then diffuse into the interspace between TiO₂ NWs and adhere to the surface of TiO₂ NWs, while in the meantime they polymerize into g-CNQD. After the deposition, the color of the FTO substrates with TiO₂ NWs turned from white to yellow (Figure S1b), in accordance with the color of g-C₃N₄. Scanning electron microscopy (SEM) images show that the perpendicular TiO₂ NW arrays uniformly grow on the whole substrate with diameters of $\sim 150 \text{ nm}$ and lengths of $1.5\text{--}2 \mu\text{m}$ (Figure 2a,b). After decorating with g-CNQDs, there is no significant morphology difference compared to pristine TiO₂ NWs, except for slight aggregation between adjacent nanowires (Figure 2c). Transmission electron microscopy (TEM) images show that the obtained TiO₂ NWs are single-crystalline and covered by a thin layer of nanoparticles with an average diameter of $\sim 5 \pm 2 \text{ nm}$ (Figure 2d). High-resolution TEM (HRTEM) images reveal that the crystal lattice spacing of the quantum dots is about 0.336 nm (Figure 2e), which corresponds to the (002) crystal plane of g-C₃N₄.³⁰ The lattice distances of 0.324 , 0.148 , and 0.249 nm in the trunk NWs are correlated to the (110), (002), and (101) crystal planes of rutile TiO₂.²⁸ The elemental mapping of a representative g-CNQD-decorated TiO₂ NW confirms that both C and N elements are uniformly distributed all over the whole structure (Figure S2), indicating that g-CNQDs are successfully incorporated with TiO₂ NWs. The atom ratio of C and Ti is calculated as 3.6:31.4, according to the EDX results. Furthermore, the solution with well-dispersed g-CNQDs can be obtained by immersing FTO substrates with g-CNQD-decorated TiO₂ NWs under sonication. The single g-CNQD displays an average size of $\sim 5 \text{ nm}$ and clear lattice fringes (Figure 2f and inset), suggesting the

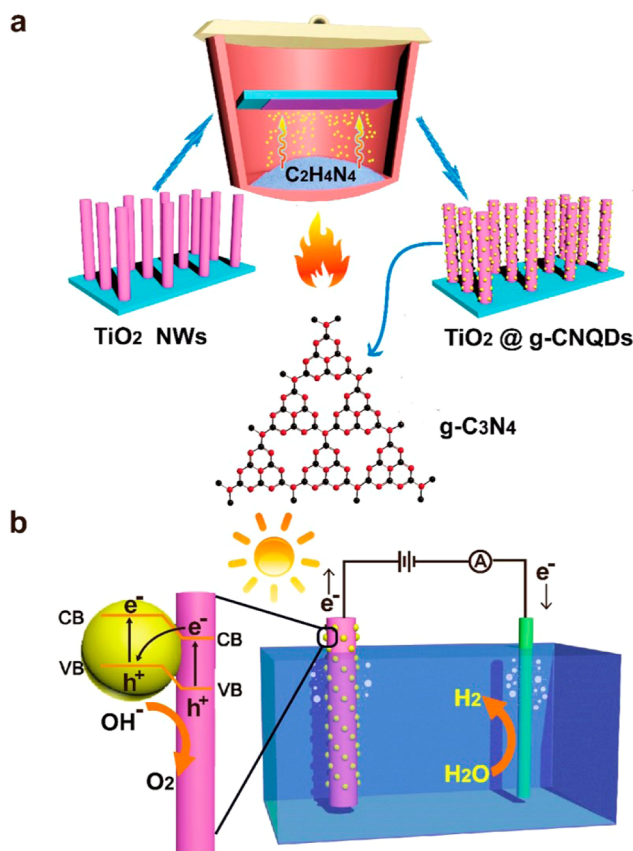


Figure 1. (a) Schematic illustration of the CVD process for the synthesis of g-CNQDs on TiO₂ NWs in an aluminum crucible device. (b) Schematic illustration of the energy diagrams and photoelectrochemical system of the TiO₂@g-CNQD NWs.

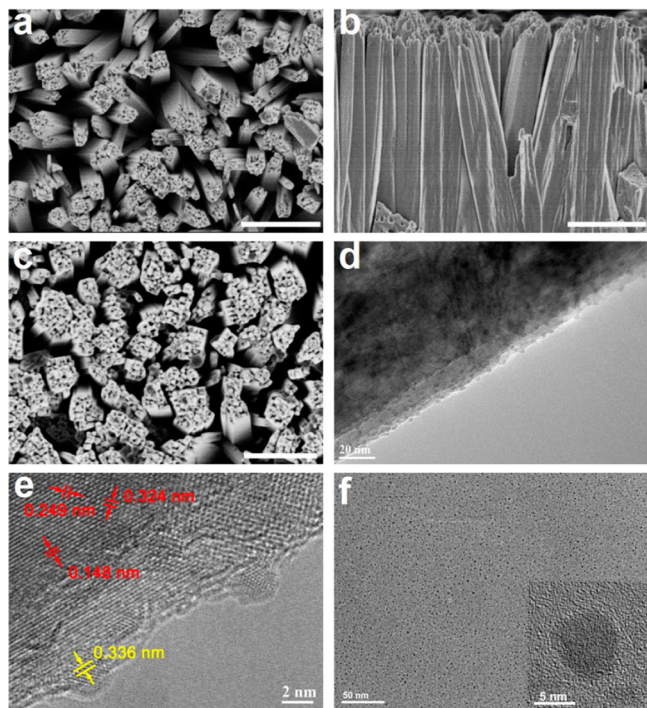


Figure 2. (a–c) SEM images of as-synthesized TiO_2 nanostructure. (a) Top view and (b) side view of pristine TiO_2 NWs. (c) Top view of $\text{TiO}_2@g\text{-CNQD}$ NWs (scale bars are 500 nm). (d) TEM and (e) HRTEM images of the $\text{TiO}_2@g\text{-CNQD}$ NWs. (f) TEM image of g-CNQDs dispersed in ethanol (inset: a single g-CNQD).

crystalline structures of the g-CNQDs, similar to other carbon-based quantum dot materials.³¹

X-ray diffraction (XRD) was carried out to study the phase purity of the obtained $\text{TiO}_2@g\text{-CNQD}$ composite, which clearly demonstrated the coexistence of both TiO_2 NWs and g-CNQDs (Figure 3a). The peaks at 36.3° and 62.4° are corresponding to the (101) and (002) crystal planes of rutile phase (JCPDS 21-1276),²⁸ while the peaks at 13.1° and 27.3° are attributed by the interplanar separation (100) and interlayer stacking of aromatic systems (002) of g-C₃N₄ (JCPDS 87-1526).^{3,4} Those XRD results are consistent with the lattice fringes observed in HRTEM images. Raman spectra display the peaks at 236.4, 446.8, and 609.1 cm^{-1} of TiO_2 NWs, which are well matched with rutile TiO_2 .³² The Raman peaks of $\text{TiO}_2@g\text{-CNQD}$ are similar to those of TiO_2 with a slight red shift, which can also be found in other TiO_2 -based heterostructures,³³ suggesting close contact between TiO_2 and g-CNQD (Figure 3b). A broad peak between 1000 and 2000 cm^{-1} is also observed for the $\text{TiO}_2@g\text{-CNQD}$ NWs, which is similar to bulk g-C₃N₄ as well as the previous literature.³⁴ Fourier transform infrared (FTIR) spectroscopy was also carried out to investigate the chemical composition of the obtained composite (Figure S3). The broad range of TiO_2 below 1000 cm^{-1} can be ascribed to the stretching vibration of Ti–O–Ti, and there is no significant absorption above 1000 cm^{-1} .²⁹ For the $\text{TiO}_2@g\text{-CNQD}$ NWs, several sharp absorption peaks between 950 and 1700 cm^{-1} are correlated to the stretching modes of aromatic C–N,²³ which are also consistent with those peaks of pure g-C₃N₄. In addition, the peaks for tri-s-triazine in $\text{TiO}_2@g\text{-CNQD}$ NWs are also observed.

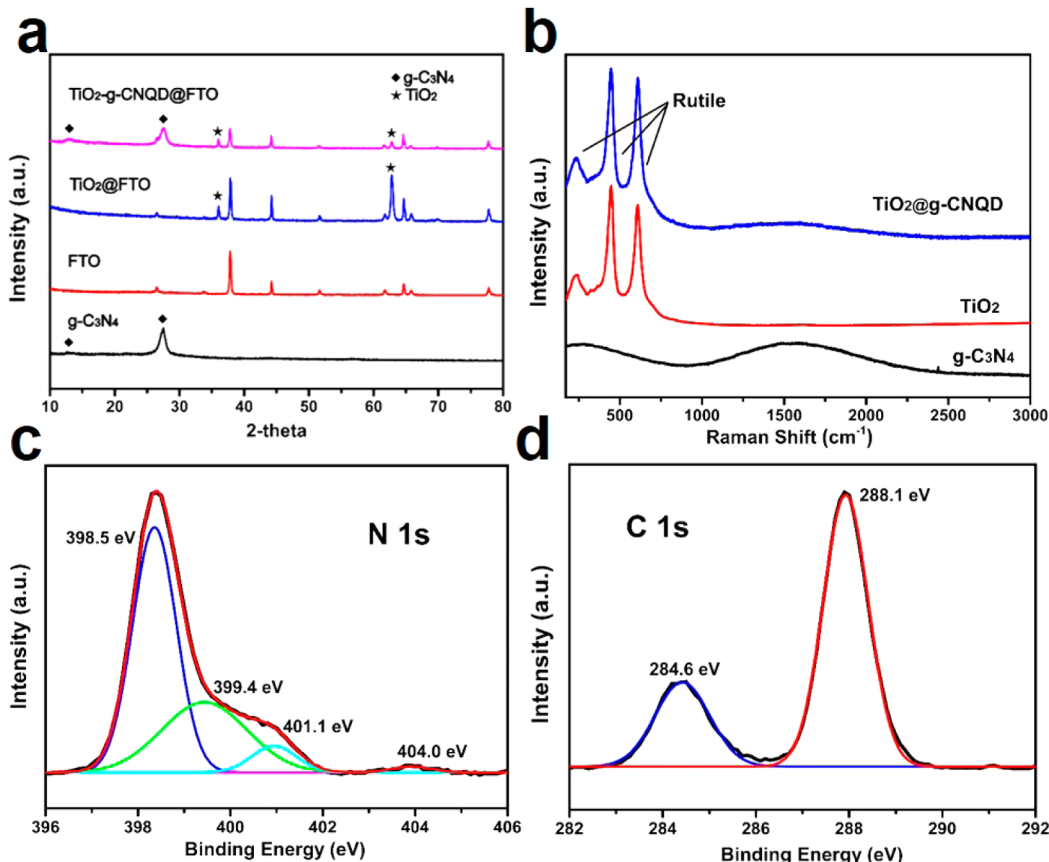


Figure 3. Structure characterization. (a) XRD patterns of bulk g-C₃N₄, blank FTO substrate, TiO_2 NWs, and $\text{TiO}_2@g\text{-CNQD}$ NWs on FTO substrates. (b) Raman spectra of bulk g-C₃N₄, TiO_2 NWs, and $\text{TiO}_2@g\text{-CNQD}$ NWs. (c) High resolution XPS spectra of (c) N 1s and (d) C 1s.

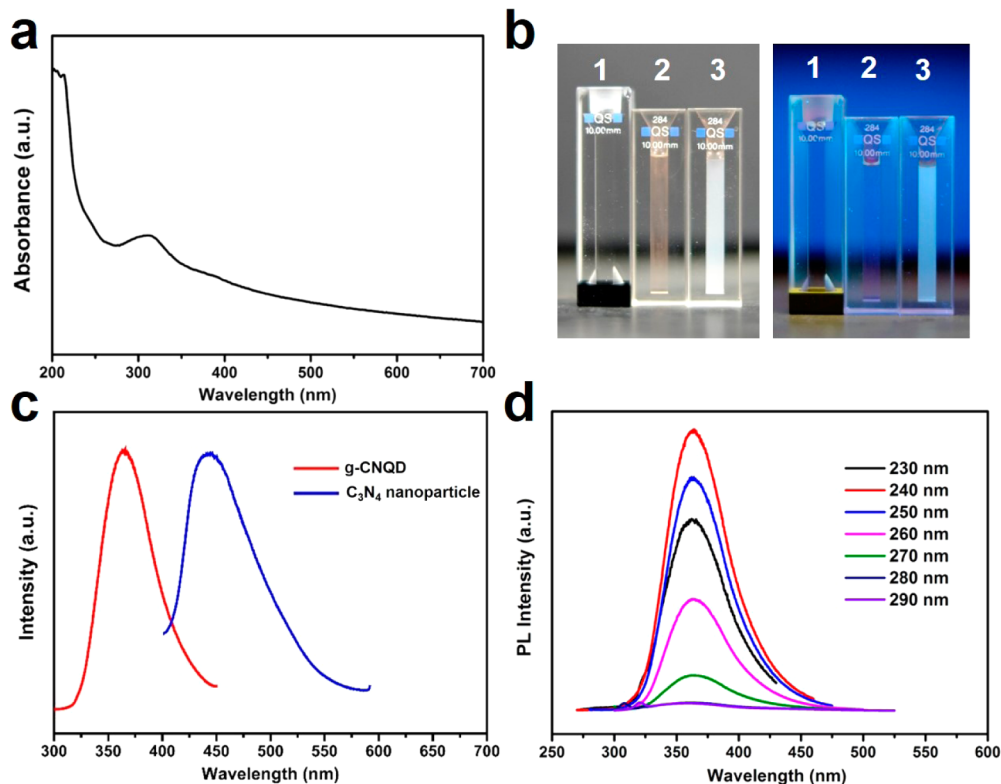


Figure 4. (a) UV–vis absorption of the mixture of g-CNQDs and C₃N₄ nanoparticles. (b) Digital photographs: pure water (1), g-CNQDs (2), and mixture of g-CNQDs and C₃N₄ nanoparticles (3) under ambient light (left) and UV irradiations (right). (c) PL spectra of pure g-CNQDs (red curve) and C₃N₄ nanoparticles (blue curve). (d) PL spectra of pure g-CNQDs excited under different wavelengths.

CNQD seem negligible compared to pure g-C₃N₄. It was likely covered by a wide absorption band of TiO₂, the amount of which was much higher than g-CNQD.

In addition, X-ray photoelectron spectroscopy (XPS) measurement was also applied to investigate the surface chemical states of the TiO₂@g-CNQD NWs. The full survey spectrum of TiO₂@g-CNQD indicates the coexistence of the elements of Ti, O, C, and N (Figure S4a). A high resolution XPS spectrum of Ti 2p shows two different peaks centered at binding energies of 457.3 and 463.5 eV, which are assigned to Ti 2p_{3/2} and Ti 2p_{1/2}. The O 1s peak at 529.5 eV is assigned to the Ti–O–Ti linkages in TiO₂ (Figure S4b,c), consistent with the XPS data of TiO₂ reported previously.²⁹ The XPS spectrum of the N 1s region can be divided into four peaks located at 398.5, 399.4, 401.1, and 404.0 eV (Figure 3c), which are ascribed to the sp²-bonded nitrogen (C=N=C), nitrogen in tertiary N–(C)₃ groups, amino groups (C–N–H), and the π excitation of the C=N conjugated structure, respectively.^{35,36}

As shown in the C 1s XPS spectrum (Figure 3d), the peak at 284.6 eV is the signal of sp²-bonded carbon in C–C, whereas the second peak located at 288.1 eV indicates the formation of N=C=N.³⁴ Furthermore, we have carried out XPS experiments for pure TiO₂ and g-C₃N₄ for comparison (Figure S5), those results were similar to TiO₂@g-CNQD with a slight difference, also suggesting the interaction between TiO₂ and g-CNQD.

The photoluminescence property of g-CNQDs was first characterized and investigated in water by immersing several growth substrates with TiO₂@g-CNQD NWs with 10 min sonication. The UV–vis spectrum in Figure 4a shows an absorption band at ~330 nm and an absorption edge at ~250 nm, as well as a rising baseline around 450 nm, indicating that

the obtained solution (Figure 4b, left 3) after sonication is a mixture of g-CNQDs and a small amount of nanostructured g-C₃N₄ (~100 nm, described as C₃N₄ nanoparticle),²³ and the bandgap of g-CNQD is about 4.59 eV according to the absorption edge, similar to the previous report.³⁷ After the nanostructured g-C₃N₄ was filtered, the solution became almost transparent (Figure 4b, left 2), which is consistent with related literature.³⁷ Under UV illumination, the g-CNQD solution (Figure 4b, right 2) is almost the same as pure water (Figure 4b, right 1), while the mixture of g-CNQD and C₃N₄ nanoparticle shows blue light (Figure 4b, right 3). Those results are consistent with PL spectra in Figure 4c, while the g-CNQD solution shows an emission peak at ~365 nm (UV light) compared to the solution with nanostructured g-C₃N₄ at ~450 nm (blue), consistent with the literature reported before.²³ In addition, the PL spectra of g-CNQDs excited under a series of wavelengths are also displayed (Figure 4d), confirming their excellent PL properties.

The combination of TiO₂ NWs and g-CNQD provides attractive features in PEC performances, compared to single components. The photocurrent measurements were carried out in the potential window of -1 to +1 V vs Ag/AgCl (i.e., 0–2 V vs reversible hydrogen electrode, RHE) in 1 M KOH electrolyte under simulated solar light with chopped on–off cycles (Figure 5a). At 0 V vs Ag/AgCl, the photocurrent densities of the pristine TiO₂ NWs and TiO₂@g-CNQD NWs are 1.36 and 3.40 mA/cm², respectively. The 2.5 times enhancement indicates that g-CNQD has a significant sensitization effect on TiO₂ NWs, mainly attributed to the enhanced photoabsorption of g-CNQD and better charge separation. From the digital photograph that shows the TiO₂@g-CNQD electrode as a photoanode, a substantial amount of

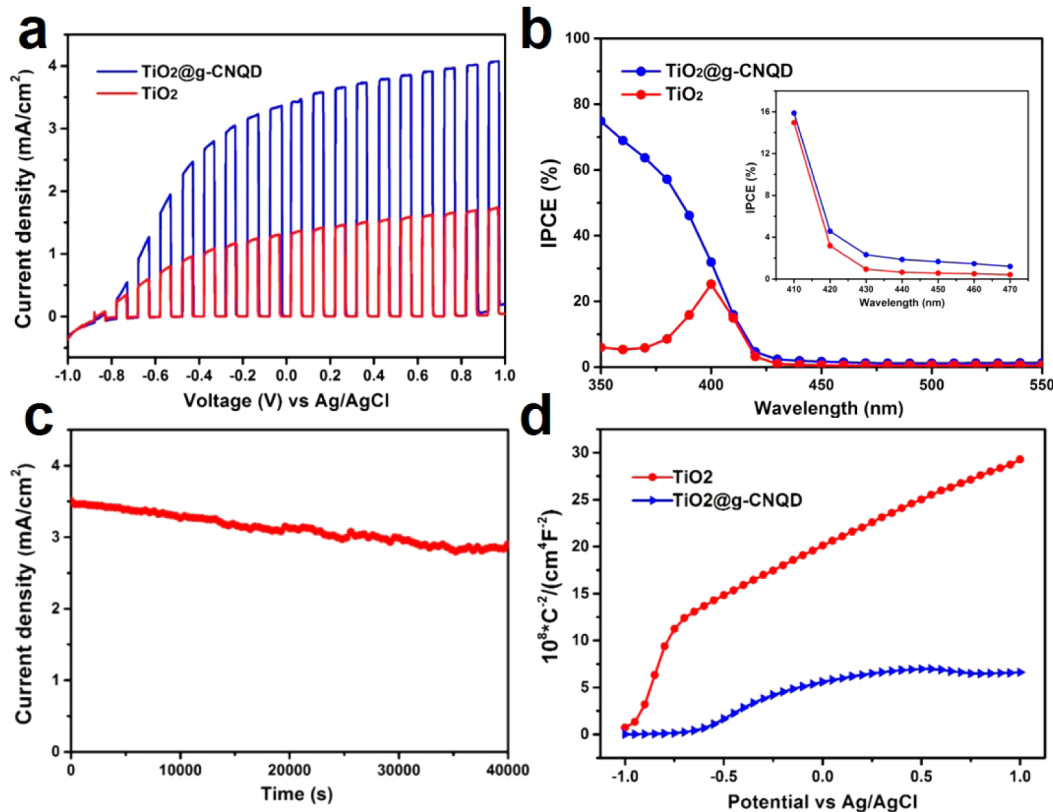


Figure 5. Photoelectrochemical measurements. (a) Photocurrent density of the pristine TiO_2 NW (red curve) and $\text{TiO}_2@g\text{-CNQD}$ NW (blue curve) photoanodes at repeated on/off cycles of simulated sunlight illumination. (b) IPCE curves of the pristine TiO_2 NWs (red curve) and $\text{TiO}_2@g\text{-CNQD}$ (blue curve). (c) Time-dependent photocurrent density of the $\text{TiO}_2@g\text{-CNQD}$ NW photoanode under continuous simulated sunlight illumination. (d) Mott–Schottky plots of pristine TiO_2 NWs and $\text{TiO}_2@g\text{-CNQD}$ NWs.

H_2 bubbles were produced on the Pt counter electrode under light irradiation (Figure S6). The incident-photon-to-current conversion efficiency (IPCE) measurement taken at 0 V vs Ag/AgCl shows that the pristine TiO_2 NWs have IPCE values of between 10% and 20% from 350 to 400 nm, with a maximum value of ~26% at ~400 nm, and they drop sharply to almost negligible in the visible region (after subtracting dark current). As for the $\text{TiO}_2@g\text{-CNQD}$ NWs, there is a remarkable improvement in the UV region, and the IPCE can be as high as 75% around 350 nm (Figure 5b). In addition, there is also a small improvement in the visible region from 420 to 450 nm (Figure 5b inset), consistent with the rising baseline in the liquid UV-vis spectrum in Figure 4a, which is contributed mostly by the C_3N_4 nanoparticles. By integrating the IPCE spectra with the solar spectrum according to a previous report,²⁴ we can also obtain photocurrent densities similar to J – V curves, confirming the accuracy of the results. In addition, we carried out the solid UV-vis absorption spectrum of the $\text{TiO}_2@g\text{-CNQD}$ composites, which also shows an enhanced absorption in the UV region as well as an increase in the visible region (Figure S7). Furthermore, the $\text{TiO}_2@g\text{-CNQD}$ NWs possess excellent stability (Figure 4c), as the photocurrent remains relatively stable and retains ~82% of its original value after more than 10 h of continuous testing under simulated solar light at 0 V vs Ag/AgCl. The same test has also been carried out for pure TiO_2 NWs (Figure S8), and the photocurrent retains 79% under the same duration.³⁸ The outstanding PEC performance stems from the optimized $\text{TiO}_2/g\text{-C}_3\text{N}_4$ heterojunction structure, in which the graphene-like structure of $\text{g-C}_3\text{N}_4$ enhances the photoabsorption as well as

facilitates the charge separation between TiO_2 NWs and g-CNQDs .

To demonstrate the charge transport behaviors of $\text{TiO}_2@g\text{-CNQD}$ NWs versus pristine TiO_2 NWs, the Mott–Schottky measurement was carried out to investigate the charge carrier density of the interface between semiconductor electrode and electrolyte (Figure 4d). Both samples show positive slopes, indicating the pristine TiO_2 and $\text{TiO}_2@g\text{-CNQD}$ NWs are n-type semiconductors.³⁹ According to the Mott–Schottky equation,⁴⁰ the $\text{TiO}_2@g\text{-CNQD}$ NWs show a much smaller slope than that of pristine TiO_2 NWs, indicating significantly higher charge carrier densities. The flat band potential (E_{FB}) values of the pristine TiO_2 and $\text{TiO}_2@g\text{-CNQD}$ NWs are −0.95 and −0.85 V, respectively.⁴¹ The positive shifts of E_{FB} for $\text{TiO}_2@g\text{-CNQD}$ in comparison with TiO_2 suggests a decrease in the bending of band edges, which is attributed to the increased material/electrolyte interface for the PEC reaction that can improve the charge carrier transfer efficiency. Those results are consistent with Figure 1b, and a similar transition of the Mott–Schottky measurement has been observed in a previous report of Pd quantum-dot-sensitized TiO_2 nanotubes.⁴² Thus, it can be concluded that the g-CNQD decoration can distinctly facilitate the formation of space charge layers, resulting in better PEC performance.

To study the interfacial effect of the $\text{TiO}_2@g\text{-CNQD}$ NWs, density functional theory (DFT) calculations were carried out on the basis of an atomic model built by adding $\text{g-C}_3\text{N}_4$ on top of the TiO_2 (110) surface (Figure 6a). Structure optimization was performed for the $\text{TiO}_2/g\text{-C}_3\text{N}_4$ interface structure using the conjugate gradient method (Methods in the Supporting

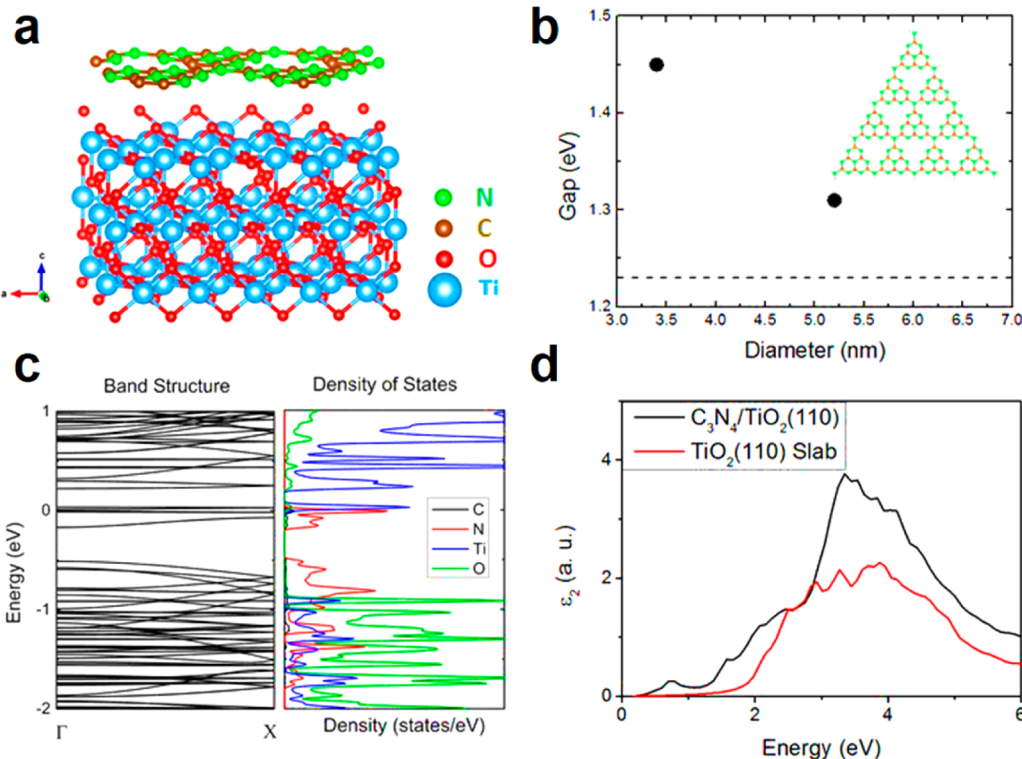


Figure 6. (a) Structure model for computational simulation of the interface between g-C₃N₄ and the rutile TiO₂ (110) surface. The green, brown, red, and blue spheres represent N, C, O, and Ti atoms, respectively. (b) HOMO–LUMO gap dependence of the size of g-CNQDs. The dashed line indicates the band gap of a g-C₃N₄ monolayer. (c) Band structure and partial density of states of the g-C₃N₄/TiO₂ (110) interface. (d) Calculated imaginary part of the dielectric function of the g-C₃N₄/TiO₂ (110) interface (black line) and the rutile (110) surface (red line).

Information). The equilibrium distance between the graphene layer and the top of the TiO₂ was calculated to be 0.323 nm. The average charge transfer was analyzed based on the Bader method.⁴³ For the TiO₂/g-C₃N₄ interface, there is an average charge transfer of about 0.007 e per atom from g-C₃N₄ to TiO₂, which results in small increase of charge carrier in TiO₂ nanowires.

Because the band gap of g-C₃N₄ is more suitable for solar absorption, the g-C₃N₄/TiO₂ is also expected to exhibit better photocatalytic activities under visible light, as demonstrated in some other systems.⁴⁴ Here, the size effect of the synthesized g-CNQDs may open the HOMO–LUMO gap. The gap of g-CNQD with diameters of ~5 nm was calculated, which is ~0.1 eV larger than that of the g-C₃N₄ monolayer (Figure 6b). The widening of the HOMO–LUMO gap by the quantum confinement effect can result in a blue shift in the absorption spectra. To further study the enhancement of PEC performance of the system, the electronic structure properties were calculated and displayed (Figure 6c). From the calculation of the partial density of states, the basic electronic structure of TiO₂ remains unchanged, but new electronic levels in the intrinsic band gap of TiO₂ appear, which is mainly contributed by N atoms of the g-C₃N₄ layer, even without N doping in TiO₂. As a consequence, with the formation of intermediate bands, the intrinsic band gap is narrowed, which is similar to the n–p codoping effect.⁴⁵ To illustrate such an effect, the imaginary part of the dielectric function for the TiO₂/g-C₃N₄ (110) interface and the pure TiO₂ (110) surface was calculated (Figure 6d). The optical absorption of the pure TiO₂ slab occurs only in the UV region, though the Perdew–Burke–Ernzerhof (PBE) functional underestimates the band gap,

which results in a red shift of ~1.0 eV.⁴⁶ Under the same shift, the hybrid TiO₂/g-C₃N₄ system has optical absorption in the visible region and displays better photocatalytic activities under the UV region.

CONCLUSION

In summary, we have successfully developed a synthetic approach for g-CNQD through a facile and simple quasi-CVD method, and TiO₂ NW arrays were used to facilitate the g-CNQD deposition and serve as a semiconductor photoanode material. The whole reaction can be facilely performed in a homemade aluminum crucible under a semiclosed environment. The PEC performance of the heterojunctioned TiO₂@g-CNQD NWs was significantly improved, especially in the UV region, with 2.5 times the photocurrent enhancement at 0 V applied potential vs Ag/AgCl under simulated solar light. This optimized PEC performance is attributed to g-CNQD in enhancement of both photoabsorption and charge transport behaviors. Moreover, DFT calculations were carried out to elucidate the synergistic effect of TiO₂ and g-C₃N₄. The as-synthesized g-CNQD with uniform size shows typical characteristics of carbon-based QDs but also distinct and outstanding photoluminescence properties. Our method suggests an alternative approach to combine g-C₃N₄ QDs with semiconductor nanowire structures, which can also be extended to prepare other g-C₃N₄-semiconductor composite nanostructures.

ASSOCIATED CONTENT**Supporting Information**

The Supporting Information is available free of charge on the ACS Publications website at DOI: [10.1021/acsami.6b01534](https://doi.org/10.1021/acsami.6b01534).

Detailed experimental section and additional figures (PDF)

AUTHOR INFORMATION**Corresponding Authors**

*E-mail: zhanglijuan@fudan.edu.cn.

*E-mail: gzheng@fudan.edu.cn.

Author Contributions

¹T.A. and J.T. contributed equally to this work. The manuscript was written through contributions of all authors. All authors have given approval to the final version of the manuscript.

Notes

The authors declare no competing financial interest.

ACKNOWLEDGMENTS

We thank the following funding agencies for supporting this work: the National Key Basic Research Program of China (2013CB934104), the Natural Science Foundation of China (21322311, 21473038, 21471034), the Science and Technology Commission of Shanghai Municipality (14JC1490500), the Program for Professor of Special Appointment (Eastern Scholar) at Shanghai Institutions of Higher Learning, and the Collaborative Innovation Center of Chemistry for Energy Materials (2011-iChem). The authors extend their sincere appreciation to the Deanship of Scientific Research at King Saud University for funding the Prolific Research group (PRG-1436-14).

REFERENCES

- (1) Wang, X. C.; Maeda, K.; Thomas, A.; Takanabe, K.; Xin, G.; Carlsson, J. M.; Domen, K.; Antonietti, M. A Metal-free Polymeric Photocatalyst for Hydrogen Production from Water under Visible Light. *Nat. Mater.* **2009**, *8*, 76–80.
- (2) Liu, J.; Liu, Y.; Liu, N. Y.; Han, Y. Z.; Zhang, X.; Huang, H.; Lifshitz, Y.; Lee, S.-T.; Zhong, J.; Kang, Z. H. Metal-free Efficient Photocatalyst for Stable Visible Water Splitting via a Two-electron Pathway. *Science* **2015**, *347*, 970–974.
- (3) Cao, S. W.; Low, J.; Yu, J. G.; Jaroniec, M. Polymeric Photocatalysts Based on Graphitic Carbon Nitride. *Adv. Mater.* **2015**, *27*, 2150–2176.
- (4) Zheng, Y.; Lin, L. H.; Wang, B.; Wang, X. C. Graphitic Carbon Nitride Polymers toward Sustainable Photoredox Catalysis. *Angew. Chem., Int. Ed.* **2015**, *54*, 12868–12884.
- (5) Tay, Q.; Kanhere, P.; Ng, C. F.; Chen, S.; Chakraborty, S.; Huan, A. C. H.; Sum, T. C.; Ahuja, R.; Chen, Z. Defect Engineered g-C₃N₄ for Efficient Visible Light Photocatalytic Hydrogen Production. *Chem. Mater.* **2015**, *27*, 4930–4933.
- (6) Li, X. B.; Hartley, G.; Ward, A. J.; Young, P. A.; Masters, A. F.; Maschmeyer, T. Hydrogenated Defects in Graphitic Carbon Nitride Nanosheets for Improved Photocatalytic Hydrogen Evolution. *J. Phys. Chem. C* **2015**, *119*, 14938–14946.
- (7) Niu, P.; Zhang, L. L.; Liu, G.; Cheng, H.-M. Graphene-Like Carbon Nitride Nanosheets for Improved Photocatalytic Activities. *Adv. Funct. Mater.* **2012**, *22*, 4763–4770.
- (8) Duan, J. J.; Chen, S.; Jaroniec, M.; Qiao, S. Z. Porous C₃N₄ Nanolayers@N-Graphene Films as Catalyst Electrodes for Highly Efficient Hydrogen Evolution. *ACS Nano* **2015**, *9*, 931–940.
- (9) Han, Q.; Wang, B.; Gao, J.; Cheng, Z. H.; Zhao, Y.; Zhang, Z. P.; Qu, L. T. Atomically Thin Mesoporous Nanomesh of Graphitic C₃N₄ for High-Efficiency Photocatalytic Hydrogen Evolution. *ACS Nano* **2016**, *10*, 2745–2751.
- (10) Jun, Y.-S.; Lee, E. Z.; Wang, X. C.; Hong, W. H.; Stucky, G. D.; Thomas, A. From Melamine-Cyanuric Acid Supramolecular Aggregates to Carbon Nitride Hollow Spheres. *Adv. Funct. Mater.* **2013**, *23*, 3661–3667.
- (11) Zhang, J. S.; Zhang, M. W.; Yang, C.; Wang, X. C. Nanospherical Carbon Nitride Frameworks with Sharp Edges Accelerating Charge Collection and Separation at a Soft Photocatalytic Interface. *Adv. Mater.* **2014**, *26*, 4121–4126.
- (12) Xu, Y. L.; Niu, X. Y.; Zhang, H. J.; Xu, L. F.; Zhao, S. G.; Chen, H. L.; Chen, X. G. Switch-on Fluorescence Sensing of Glutathione in Food Samples Based on a Graphitic Carbon Nitride Quantum Dot (g-CNQD)-Hg²⁺ Chemosensor. *J. Agric. Food Chem.* **2015**, *63*, 1747–1755.
- (13) Bhunia, M. K.; Melissen, S.; Parida, M. R.; Sarawade, P.; Basset, J.-M.; Anjum, D. H.; Mohammed, O. F.; Sautet, P.; Le Bahers, T.; Takanabe, K. Dendritic Tip-on Polytriazine-Based Carbon Nitride Photocatalyst with High Hydrogen Evolution Activity. *Chem. Mater.* **2015**, *27*, 8237–8247.
- (14) Bojdys, M. J.; Severin, N.; Rabe, J. P.; Cooper, A. I.; Thomas, A.; Antonietti, M. Exfoliation of Crystalline 2D Carbon Nitride: Thin Sheets, Scrolls and Bundles via Mechanical and Chemical Routes. *Macromol. Rapid Commun.* **2013**, *34*, 850–854.
- (15) Ma, T. Y.; Tang, Y. H.; Dai, S.; Qiao, S. Z. Proton-Functionalized Two-Dimensional Graphitic Carbon Nitride Nano-sheet: An Excellent Metal-/Label-Free Biosensing Platform. *Small* **2014**, *10*, 2382–2389.
- (16) Zhang, J. S.; Guo, F. S.; Wang, X. C. An Optimized and General Synthetic Strategy for Fabrication of Polymeric Carbon Nitride Nanoarchitectures. *Adv. Funct. Mater.* **2013**, *23*, 3008–3014.
- (17) Yan, H. J. Soft-templating Synthesis of Mesoporous Graphitic Carbon Nitride with Enhanced Photocatalytic H₂ Evolution under Visible Light. *Chem. Commun.* **2012**, *48*, 3430–3432.
- (18) Zhu, S. J.; Meng, Q. N.; Wang, L.; Zhang, J. H.; Song, Y. B.; Jin, H.; Zhang, K.; Sun, H. C.; Wang, H. Y.; Yang, B. Highly Photoluminescent Carbon Dots for Multicolor Patterning, Sensors, and Bioimaging. *Angew. Chem., Int. Ed.* **2013**, *52*, 3953–3957.
- (19) Bian, J. C.; Huang, C.; Wang, L. Y.; Hung, T.; Daoud, W. A.; Zhang, R. Q. Carbon Dot Loading and TiO₂ Nanorod Length Dependence of Photoelectrochemical Properties in Carbon Dot/TiO₂ Nanorod Array Nanocomposites. *ACS Appl. Mater. Interfaces* **2014**, *6*, 4883–4890.
- (20) Chao, D. L.; Zhu, C. R.; Xia, X. H.; Liu, J. L.; Zhang, X.; Wang, J.; Liang, P.; Lin, J. Y.; Zhang, H.; Shen, Z. X.; Fan, H. J. Graphene Quantum Dots Coated VO₂ Arrays for Highly Durable Electrodes for Li and Na Ion Batteries. *Nano Lett.* **2015**, *15*, 565–573.
- (21) Li, H. T.; Zhang, X. Y.; MacFarlane, D. R. Carbon Quantum Dots/Cu₂O Heterostructures for Solar-Light-Driven Conversion of CO₂ to Methanol. *Adv. Energy Mater.* **2015**, *5*, 1401077.
- (22) Zhang, X. D.; Wang, H. X.; Wang, H.; Zhang, Q.; Xie, J. F.; Tian, Y. P.; Wang, J.; Xie, Y. Single-Layered Graphitic-C₃N₄ Quantum Dots for Two-Photon Fluorescence Imaging of Cellular Nucleus. *Adv. Mater.* **2014**, *26*, 4438–4443.
- (23) Zhou, Z. X.; Shen, Y. F.; Li, Y.; Liu, A. R.; Liu, S. Q.; Zhang, Y. J. Chemical Cleavage of Layered Carbon Nitride with Enhanced Photoluminescent Performances and Photoconduction. *ACS Nano* **2015**, *9*, 12480–12487.
- (24) Wang, G. M.; Xiao, X. H.; Li, W. Q.; Lin, Z. Y.; Zhao, Z. P.; Chen, C.; Wang, C.; Li, Y. J.; Huang, X. Q.; Miao, L.; Jiang, C. Z.; Huang, Y.; Duan, X. F. Significantly Enhanced Visible Light Photoelectrochemical Activity in TiO₂ Nanowire Arrays by Nitrogen Implantation. *Nano Lett.* **2015**, *15*, 4692–4698.
- (25) Tang, J.; Zhang, Y. Y.; Kong, B.; Wang, Y. C.; Da, P. M.; Li, J.; Elzatahry, A. A.; Zhao, D. Y.; Gong, X. G.; Zheng, G. F. Solar-Driven Photoelectrochemical Probing of Nanodot/Nanowire/Cell Interface. *Nano Lett.* **2014**, *14*, 2702–2708.
- (26) Meng, J. X.; Zhang, P. C.; Zhang, F. L.; Liu, H. L.; Fan, J. B.; Liu, X. L.; Yang, G.; Jiang, L.; Wang, S. T. A Self-Cleaning TiO₂

- Nanosisal-like Coating toward Disposing Nanobiochips of Cancer Detection. *ACS Nano* **2015**, *9*, 9284–9291.
- (27) Kondo, K.; Murakami, N.; Ye, C.; Tsubota, T.; Ohno, T. Development of Highly Efficient Sulfur-doped TiO_2 Photocatalysts Hybridized with Graphitic Carbon Nitride. *Appl. Catal., B* **2013**, *142*–*143*, 362–367.
- (28) Tang, J.; Kong, B.; Wang, Y. C.; Xu, M.; Wang, Y. L.; Wu, H.; Zheng, G. F. Photoelectrochemical Detection of Glutathione by IrO_2 -Hemin- TiO_2 Nanowire Arrays. *Nano Lett.* **2013**, *13*, 5350–5354.
- (29) Li, Y. G.; Wang, R. R.; Li, H. J.; Wei, X. L.; Feng, J.; Liu, K. Q.; Dang, Y. Q.; Zhou, A. N. Efficient and Stable Photoelectrochemical Seawater Splitting with $\text{TiO}_2@g\text{-C}_3\text{N}_4$ Nanorod Arrays Decorated by Co-Pt. *J. Phys. Chem. C* **2015**, *119*, 20283–20292.
- (30) Li, K.; Gao, S. M.; Wang, Q. Y.; Xu, H.; Wang, Z. Y.; Huang, B. B.; Dai, Y.; Lu, J. In-Situ-Reduced Synthesis of Ti^{3+} Self-doped $\text{TiO}_2/g\text{-C}_3\text{N}_4$ Heterojunctions with High Photocatalytic Performance under LED Light Irradiation. *ACS Appl. Mater. Interfaces* **2015**, *7*, 9023–9030.
- (31) Oh, Y.; Le, V.-D.; Maiti, U. N.; Hwang, J. O.; Park, W. J.; Lim, J.; Lee, K. E.; Bae, Y.-S.; Kim, Y.-H.; Kim, S. O. Selective and Regenerative Carbon Dioxide Capture by Highly Polarizing Porous Carbon Nitride. *ACS Nano* **2015**, *9*, 9148–9157.
- (32) Li, R. G.; Weng, Y. X.; Zhou, X.; Wang, X. L.; Mi, Y.; Chong, R. F.; Han, H. X.; Li, C. Achieving Overall Water Splitting using Titanium Dioxide-based Photocatalysts of Different Phases. *Energy Environ. Sci.* **2015**, *8*, 2377–2382.
- (33) Zhou, X.; Häublein, V.; Liu, N.; Nguyen, N. T.; Zolnhofer, E. M.; Tsuchiya, H.; Killian, M. S.; Meyer, K.; Frey, L.; Schmuki, P. TiO_2 Nanotubes: Nitrogen-Ion Implantation at Low Dose Provides Noble-Metal-Free Photocatalytic H_2 -Evolution Activity. *Angew. Chem., Int. Ed.* **2016**, *55*, 3763–3767.
- (34) Kang, Y. Y.; Yang, Y. Q.; Yin, L.-C.; Kang, X. D.; Liu, G.; Cheng, H.-M. An Amorphous Carbon Nitride Photocatalyst with Greatly Extended Visible-Light-Responsive Range for Photocatalytic Hydrogen Generation. *Adv. Mater.* **2015**, *27*, 4572–4577.
- (35) Liang, Q. H.; Li, Z.; Yu, X. L.; Huang, Z.-H.; Kang, F. Y.; Yang, Q.-H. Macroscopic 3D Porous Graphitic Carbon Nitride Monolith for Enhanced Photocatalytic Hydrogen Evolution. *Adv. Mater.* **2015**, *27*, 4634–4639.
- (36) Jiang, Z. F.; Zhu, C. Z.; Wan, W. M.; Qian, K.; Xie, J. M. Constructing Graphite-like Carbon Nitride Modified Hierarchical Yolk-shell TiO_2 Spheres for Water Pollution Treatment and Hydrogen Production. *J. Mater. Chem. A* **2016**, *4*, 1806–1818.
- (37) Song, Z. P.; Lin, T. R.; Lin, L. H.; Lin, S.; Fu, F. F.; Wang, X. C.; Guo, L. Q. Invisible Security Ink Based on Water-Soluble Graphitic Carbon Nitride Quantum Dots. *Angew. Chem., Int. Ed.* **2016**, *55*, 2773–2777.
- (38) Yang, Y.; Ling, Y. C.; Wang, G. M.; Liu, T. Y.; Wang, F. X.; Zhai, T.; Tong, Y. X.; Li, Y. Photohole Induced Corrosion of Titanium Dioxide: Mechanism and Solutions. *Nano Lett.* **2015**, *15*, 7051–7057.
- (39) Wang, Y. C.; Zhang, Y. Y.; Tang, J.; Wu, H. Y.; Xu, M.; Peng, Z.; Gong, X. G.; Zheng, G. F. Simultaneous Etching and Doping of TiO_2 Nanowire Arrays for Enhanced Photoelectrochemical Performance. *ACS Nano* **2013**, *7*, 9375–9383.
- (40) Resasco, J.; Zhang, H.; Kornienko, N.; Becknell, N.; Lee, H.; Guo, J. H.; Briseno, A. L.; Yang, P. D. $\text{TiO}_2/\text{BiVO}_4$ Nanowire Heterostructure Photoanodes Based on Type II Band Alignment. *ACS Cent. Sci.* **2016**, *2*, 80–88.
- (41) Gelderman, K.; Lee, L.; Donne, S. W. Flat-Band Potential of a Semiconductor: Using the Mott–Schottky Equation. *J. Chem. Educ.* **2007**, *84*, 685.
- (42) Ye, M. D.; Gong, J. J.; Lai, Y. K.; Lin, C. J.; Lin, Z. Q. High-Efficiency Photoelectrocatalytic Hydrogen Generation Enabled by Palladium Quantum Dots-Sensitized TiO_2 Nanotube Arrays. *J. Am. Chem. Soc.* **2012**, *134*, 15720–15723.
- (43) Tang, W.; Sanville, E.; Henkelman, G. A Grid-based Bader Analysis Algorithm without Lattice Bias. *J. Phys.: Condens. Matter* **2009**, *21*, 084204.
- (44) Du, A. J.; Ng, Y. H.; Bell, N. J.; Zhu, Z. H.; Amal, R.; Smith, S. C. Hybrid Graphene/Titania Nanocomposite: Interface Charge Transfer, Hole Doping, and Sensitization for Visible Light Response. *J. Phys. Chem. Lett.* **2011**, *2*, 894–899.
- (45) Zhu, W. G.; Qiu, X. F.; Iancu, V.; Chen, X.-Q.; Pan, H.; Wang, W.; Dimitrijevic, N. M.; Rajh, T.; Meyer, H. M.; Paranthaman, M. P.; Stocks, G. M.; Weitering, H. H.; Gu, B. H.; Eres, G.; Zhang, Z. Y. Band Gap Narrowing of Titanium Oxide Semiconductors by Non-compensated Anion-Cation Codoping for Enhanced Visible-Light Photoactivity. *Phys. Rev. Lett.* **2009**, *103*, 226401.
- (46) Coletti, C.; Riedl, C.; Lee, D. S.; Krauss, B.; Patthey, L.; von Klitzing, K.; Smet, J. H.; Starke, U. Charge Neutrality and Band-gap Tuning of Epitaxial Graphene on SiC by Molecular Doping. *Phys. Rev. B: Condens. Matter Mater. Phys.* **2010**, *81*, 235401.